After taking the interband effects into account, we can write the precding result in the form [23, 36],

$$\varepsilon^{zz}(\omega) = \varepsilon^{zz}_{\text{inter}}(\omega) + 1 + \omega_p^2 \sum_i \sum_f \frac{S^{zz}_{i,f}}{\omega^2_{i,f} - \omega^2 - j\gamma\omega}, \tag{9}$$

where we have introduced

$$S^{zz}_{i,f} = \frac{2\mu\,\omega_{i,f}}{\hbar N} |\langle \psi_f | z | \psi_i \rangle|^2, \tag{10}$$

and $N = n_e V_p$ stands for the total number of conduction electrons within the nanoparticle. All occupied states qualify as initial states and all unoccupied states qualify as final states. It is assumed that all states below the Fermi energy of the metal are occupied while the states above are unoccupied. The electron number N equals to twice the number of occupied states because of the spin degeneracy of electrons.

Equation (9) provides the general quantum-mechanical expression for the dielectric function of a spherical dome shell. However, The double sum in this equation is not easy to perform if we note that the sum over i and f is actually over all quantum numbers needed to specify the quantum state. Thus, we adopt the following strategy. Rather than calculating the complex quantity $\varepsilon^{zz}(\omega)$, we focus on its imaginary part responsible to absorption. From Eq. (9) it can be written as,

$$[\varepsilon^{zz}(\omega)]_{\text{im}} = [\varepsilon^{zz}_{\text{inter}}(\omega)]_{\text{im}} + \omega_p^2 \sum_i \sum_f \frac{S^{zz}_{i,f}\gamma\omega}{(\omega^2_{i,f} - \omega^2)^2 + \gamma^2\omega^2}. \tag{11}$$

The real part of the dielectric function can then be calculated using the Kramers–Kronig relation [37]

$$[\varepsilon^{zz}(\omega)]_{\text{re}} = \frac{2\omega}{\pi} \text{P} \int_0^\infty \frac{[\varepsilon^{zz}(\omega')]_{\text{im}} - 1}{\omega'^2 - \omega^2} \text{d}\omega',$$

where P denotes the Cauchy principal value.

We now focus on how to perform the double sum in Eq. (11). It is known that he resonances of $[\varepsilon^{zz}(\omega)]_{\text{im}}$ occur in groups corresponding to changes in the value of the quantum number for which the energy dependence is the greatest [23, 36]. Let us call this quantum number ν and let the difference of this quantum number between the final and initial states be $\Delta\nu$. A Lorenzian profile can be fitted to $[\varepsilon^{zz}(\omega)]_{\text{im}}$ by writing $S^{zz}_{i,f}$ as a function of $\Delta\nu$ and introducing the group frequency $\Omega^{zz}_{\Delta\nu}$ as,

$$[\varepsilon^{zz}(\omega)]_{\text{im}} = [\varepsilon^{zz}_{\text{inter}}(\omega)]_{\text{im}} + \omega_p^2 \sum_{\Delta\nu} \frac{S^{zz}_{\Delta\nu}\gamma\omega}{(\Omega^{zz\,2}_{\Delta\nu} - \omega^2)^2 + \gamma^2\omega^2},$$

where

$$S^{zz}_{\Delta\nu} = \sum_{i} \sum_{\substack{f \\ \neq \Delta\nu}} S^{zz}_{i,f}, \tag{12}$$

$$\Omega^{zz}_{\Delta\nu} = \frac{1}{S^{zz}_{\Delta\nu}} \sum_{i} \sum_{\substack{f \\ \neq \Delta\nu}} S^{zz}_{i,f}\omega_{i,f}. \tag{13}$$

The summation is restricted to all other quantum numbers and their differences between initial and final states except $\Delta\nu$. This model has proven to match well with the experimental data and the extrapolated values derived from the density functional theory approach for nanospheres of diameters in the 2–10 nm range, as presented in Ref. [17]. In this paper, it is reported that there is a substantial blue shift of resonance peaks in the experimental data and the density-functional results when the diameter of nanospheres is reduced to below 10 nm. This cannot be explained by the modified Drude model but agrees well with the results derived from the analytical model based on Eq. (12).

#207917 - $15.00 USD Received 10 Mar 2014; revised 12 Apr 2014; accepted 29 Apr 2014; published 9 May 2014

3.1. *Wave function of a spherical dome shell*

In order to calculate $S^{zz}_{\Delta v}$ we have to derive expressions for the wave functions and corresponding eigenenergies for electrons inside the spherical dome shell by solving the Schrödinger equation (4).

In Ag and Au nano structures with non ultra small dimensions , the behavior of conduction electrons can be closely approximated as a free-electron gas constrained by infinite potential barriers at the boundaries of the particle.

This enables us to describe the electronic properties of the particle in terms of a single-electron wave function that extends over the entire particle and vanishes at the boundaries. Considering the symmetry of our system, it is convenient to use the spherical coordinates (r, θ, ϕ). For a spherical dome shell, the wave function $\psi(r,\theta,\phi)$ is obtained by solving

$$\frac{-\hbar^2}{2\mu}\frac{1}{r^2\sin\theta}\left[\sin\theta\frac{\partial}{\partial r}\left(r^2\frac{\partial\psi}{\partial r}\right)+\frac{\partial}{\partial\theta}\left(\sin\theta\frac{\partial\psi}{\partial\theta}\right)+\frac{1}{\sin\theta}\frac{\partial^2\psi}{\partial\phi^2}\right]+V(r)\psi=E\psi, \tag{14}$$

with the the potential energy $V(r)$ given by

$$V(r)=\begin{cases}0 & \text{if } a\le r\le b\\ \infty & \text{otherwise}\end{cases}.$$

We also need to remember that for a spherical dome shell with the cut-off angle θ' (see Fig. 1), the angle θ is restricted to lie in the range $\theta^{'}\le\theta\le\pi$. Also note that all wave functions must be orthonormal, i.e.,

$$\int\psi_\kappa(r,\theta,\phi)[\psi_\rho(r,\theta,\phi)]^* d^3V_p=\delta_{\kappa,\rho}, \tag{15}$$

where κ and ρ are labels of the quantum states, $\delta_{\kappa,\rho}$ is the Kronecker's delta function and the integration is over the entire volume of the dome shell.

We use the standard method of separation of variables and assume that the wave function $\psi(r,\theta,\phi)$ can be separated into radial[$R(r)$], azimuthal[$F(\phi)$] and polar[$Q(\theta)$] components as,

$$\psi(r,\theta,\phi)=R(r)Q(\theta)F(\phi). \tag{16}$$

Substitution of Eq. (16) into Eq. (15) leads to the expressions:

$$\int_a^b R_\kappa(r)R^*_\rho(r)r^2dr=\delta_{\kappa,\rho}$$

$$\int_0^{2\pi}\int_{\theta'}^{\pi}F_\kappa(\phi)F^*_\rho Q_\kappa(\theta)Q^*_\rho(\theta)\sin\theta\,d\theta d\phi=\delta_{\kappa,\rho}.$$

Next step is to find solutions for the radial, polar and azimuthal components of Eq. (14).

3.1.1. Radial component

We can separate the radial part from the Eq. (14) as,

$$\frac{d^2R(r)}{dr^2}+\frac{2}{r}\frac{dR(r)}{dr}+\left[\frac{2mE}{\hbar^2}-\frac{l(l+1)}{r^2}\right]R(r)=0,$$

where $a\le r\le b$ and l is the azimuthal quantum number. For a thin shell we can make the assumption $(b-a)<<a$. The solutions of this equation involve the Bessel and Neumann functions. Using their asymptotic approximations and applying the boundary and normalization

#207917 - $15.00 USD Received 10 Mar 2014; revised 12 Apr 2014; accepted 29 Apr 2014; published 9 May 2014

conditions, we find the radial part [36],

$$R(r) = \frac{1}{r}\sqrt{\frac{2}{b-a}}\sin\left[\frac{n\pi}{b-a}(r-a)\right] \tag{17}$$

and the allowed electron energy E to be

$$E_{n,l} = \frac{h^2}{2\mu}\left[\frac{n^2\pi^2}{(b-a)^2} + \frac{l^2}{a^2}\right], \tag{18}$$

with $n \geq 1$ and $l \geq 0$. From this equation it is clear that the main quantum number over which energy changes rapidly is n because $(b-a) << a$. Therefore we can associate $\Delta\nu$ in Eq. (12) with Δn.

3.1.2. Azimuthal component

The azimuthal component of the Eq. (14) can be separated as,

$$\frac{d^2F(\phi)}{d\phi^2} + m^2F(\phi) = 0, \tag{19}$$

where m is the magnetic quantum number. After considering the boundary condition

$$F(\phi) = F(\phi + 2\pi),$$

and the normalization condition, the solution to Eq. (19) is given by

$$F(\phi) = \frac{1}{\sqrt{2\pi}}\exp(jm\phi), \tag{20}$$

where $m = \{\cdots -2, -1, 0, 1, 2, \cdots\}$.

3.1.3. Polar component

The polar component of the Eq. (14) can be separated as,

$$\sin\theta\frac{d}{d\theta}\left[\sin\theta\frac{dQ}{d\theta}\right] + \left[l(l+1)\sin^2\theta - m^2\right]Q = 0, \tag{21}$$

where $\theta' \leq \theta \leq \pi$ and $Q(\theta') = 0$. Introducing $x = \cos\theta$ we can write it in the form

$$(1-x^2)\frac{d^2Q}{dx^2} - 2x\frac{dQ}{dx} + \left[l(l+1) - \frac{m^2}{1-x^2}\right]Q = 0,$$

where we introduce the boundary point $\zeta = \cos\theta'$ such that

$$-1 \leq x \leq \zeta, \qquad Q(\zeta) = 0. \tag{22}$$

Solutions of Eq. (21) are known when the shell is complete so that $\theta' = 0$ and $x = 1$. They are known as the associated Legendre polynomials defined by [35];

$$P_l^m(x) = \frac{(-1)^l}{2^l l!}(1-x^2)^{\frac{m}{2}}\frac{d^{l+m}}{dx^{l+m}}(1-x^2)^l. \tag{23}$$

Associated Legendre polynomials have following properties that are important for our derivation:

$$\int_{-1}^{1} P_l^m(x)P_{l'}^m(x)dx = \frac{2(m+l)!}{(2l+1)(l-m)!}\,\delta_{l,l'}, \tag{24}$$

#207917 - $15.00 USD Received 10 Mar 2014; revised 12 Apr 2014; accepted 29 Apr 2014; published 9 May 2014

$$(l-m)P_l^m(x) = x(2l-1)P_{l-1}^m(x) - (l+m-1)P_{l-2}^m(x), \tag{25}$$

$$P_l^{-m}(x) = (-1)^m \frac{(l-m)!}{(l+m)!} P_l^m(x). \tag{26}$$

After normalization using Eq. (24), $Q(x)$ for a complete shell is given by

$$\begin{aligned} Q(x) &= \sqrt{\frac{(2l+1)(l-m)!}{2(m+l)!}} P_l^m(x), \\ & \qquad l > 0, \quad -l \le m \le l. \end{aligned}$$

This solution is unusable for spherical dome shells for which $\theta' \neq 0$. However, for sufficiently small θ', we can define a new set of linearly shifted Associated Legendre polynomials (shifted ALP) as,

$$\widetilde{P}_l^m(x) = P_l^m(k_1 x + k_2), \tag{27}$$

where,

$$k_1 = \frac{2}{\zeta+1}, \qquad k_2 = \frac{1-\zeta}{\zeta+1}. \tag{28}$$

These shifted ALPs enable us to write $Q(x)$ after normalization as,

$$Q(x) = \sqrt{k_1 \frac{(2l+1)(l-m)!}{2(m+l)!}} \widetilde{P}_l^m(x), \qquad l > 0, \quad -l \le m \le l. \tag{29}$$

As shown in Appendix 5, this function is orthogonal over the interval [ζ,-1] while satisfying the boundary condition given in Eq. (22).

$$\int_{-1}^{\zeta} \widetilde{Q}_l^m(x) \widetilde{Q}_{l'}^m(x) dx = 1.$$

From Eqs. (23), (26), (27), and (28) we can see that $\widetilde{P}_l^m(\zeta) = P_l^m(1) = 0$ when $m \neq 0$. This satisfies the boundary condition in Eq. (22). It also sets the lower limit of l as 1 because $m = 0$ is not allowed. Further, $\widetilde{P}_l^m(x)$ obeys the recurrence relation derived in Appendix 5.

By substituting the radial, azimuthal and polar components, given by Eqs. (17), (20), (29) respectively, in Eq. (16) we obtain the wave function in the form

$$\psi_{n,l,m}(r,\theta,\phi) = \sqrt{\frac{k_1(2l+1)(l-m)!}{2\pi(b-a)(m+l)!}} \frac{1}{r} \sin\Big[\frac{n\pi}{b-a}(r-a)\Big] \widetilde{P}_l^m(\cos\theta) \exp(jm\phi),$$

where the three quantum numbers satisfy $n \ge 1,\ l \ge 1$, and $1 \le |m| \le l$.

3.2. Calculation of $S_{i,f}^{zz}$

To obtain the dielectric function, we need to find $S_{i,f}^{zz}$ given in Eq. (11) by calculating the matrix element $\langle \psi_i | z | \psi_f \rangle$, the total number of electrons N, and the frequency difference term $\omega_{i,f}$. Also we have to find the valid ranges for $n,\ l$, and m to carry out the double sum indicated in Eq. (11).

The initial state wave function $\psi_i = \psi_{n,l,m}$ depends on the three quantum numbers $n,\ l$, and m. We take the final wave function to be $\psi_f = \psi_{n+\Delta n, l+\Delta l, m+\Delta m}$ by changing these quantum numbers to $n+\Delta n$, $l+\Delta l$ and $m+\Delta m$. Using $z = r\cos(\theta)$, the matrix element $M_{if} = \langle \psi_i | z | \psi_f \rangle$ is calculated as,

$$M_{if} = \int_0^{2\pi} d\phi \int_{\theta'}^{\pi} \sin\theta d\theta \int_a^b r^2 dr\ \psi(r,\theta,\phi)_{n,l,m}\, r\cos\theta \left[\psi(r,\theta,\phi)_{n+\Delta n, l+\Delta l, m+\Delta m}\right]^* \tag{30}$$

#207917 - $15.00 USD Received 10 Mar 2014; revised 12 Apr 2014; accepted 29 Apr 2014; published 9 May 2014

The triple integral is calculated in Appendix 5 and the final result is found to be

$$M_{if} = \delta_{\Delta m,0}\Big[\sqrt{\frac{(l+1+m)(l+1-m)}{(2l+1)(2l+3)}}\frac{\delta_{\Delta l,1}}{k_1} + \sqrt{\frac{(l+m)(l-m)}{(2l-1)(2l+1)}}\frac{\delta_{\Delta l,-1}}{k_1} - \frac{k_2}{k_1}\delta_{\Delta l,0}\Big] \times \Big\{\frac{4(b-a)[(-1)^{\Delta n}-1]n(n+\Delta n)}{\pi^2(2n+\Delta n)^2\Delta n^2} + b\delta_{\Delta n,0}\Big\}.$$

To calculate $\omega_{i,f}$ we use its definition in Eq. (7). The initial energy $E_i = E_{n,l}$ is given in Eq. (18), and the final energy is given by $E_f = E_{n+\Delta n,l+\Delta l}$. Thus,

$$\omega_{i,f} = \frac{\hbar}{2\mu}\left[\frac{\Delta n(2n+\Delta n)\pi^2}{(b-a)^2} + \frac{\Delta l(2l+\Delta l+1)}{a^2}\right]. \tag{31}$$

To calculate total number of electrons, let n_f be the value of n at the Fermi level when $l = 1$, which is the minimum value that l can have. From Eq. (18) we can write Fermi energy E_{Fermi} as,

$$E_{\text{Fermi}} = \frac{\hbar^2}{2\mu}\left[\frac{n_f^2\pi^2}{(b-a)^2} + \frac{1}{a^2}\right] \approx \frac{\hbar^2}{2\mu}\left[\frac{n_f^2\pi^2}{(b-a)^2}\right],$$

where we neglected the second term by noting that $(b-a) \ll a$ for a thin shell. Since all initial states should lie below the Fermi energy level, Using $E_i \le E_{\text{Fermi}}$, we obtain the condition following upper bound for l:

$$l \le l_{\max} = \text{Int}\Big[\sqrt{(n_f^2 - n^2)}\frac{\pi a}{(b-a)}\Big],$$

where $\text{Int}(x)$ denotes the integer part of x. The total number of electrons N can now be found by summing over all occupied states such that $n \le n_f$ and $l \le l_{\max}$. After considering the spin degeneracy, we find

$$\begin{aligned} N &= \sum_{n=1}^{n_f}\sum_{l=1}^{l_{\max}}\sum_{\substack{-l\le m\le l\\ m\neq 0}} 2 \\ &= 2\sum_{n=1}^{n_f} l_{\max}(l_{\max}+1) \approx \frac{4\pi^2a^2n_f^3}{3(b-a)^2}. \end{aligned}$$

By substituting the expressions for M_{if}, $\omega_{i,f}$, and N in (10), we finally obtain

$$\begin{aligned} S_{i,f}^{zz} = S_{n,\Delta n,l,\Delta l,m,\Delta m}^{zz}\frac{3(b-a)^2}{4\pi^2a^2n_f^3}&\left[\frac{\Delta n(2n+\Delta n)\pi^2}{(b-a)^2} + \frac{\Delta l(2l+\Delta l+1)}{a^2}\right]\times \\ &\delta_{\Delta m,0}\Big[\frac{(l+1+m)(l+1-m)}{(2l+1)(2l+3)}\frac{\delta_{\Delta l,1}}{k_1^2} + \frac{(l+m)(l-m)}{(2l-1)(2l+1)}\frac{\delta_{\Delta l,-1}}{k_1^2} + \frac{k_2^2}{k_1^2}\delta_{\Delta l,0}\Big]\times \\ &\left\{\frac{16(b-a)^2[(-1)^{\Delta n}-1]^2n^2(n+\Delta n)^2}{\pi^4(2n+\Delta n)^4\Delta n^4} + b^2\delta_{\Delta n,0}\right\}. \end{aligned}$$

The appearance of several Kronecker delta functions in this equations helps us in identifying the range of Δm and Δl. Clearly, their only allowed values are $\Delta m = 0$ and $\Delta l = -1, 0, 1$. In addition, the values of n and l are limited such that $n \le \text{Int}(n_f)$ and $l \le l_{\max}$. One more requirement is that $E_f > E_{\text{Fermi}}$. From Eq. (18), we obtain

$$l > g = \text{ceil}\Big[\frac{\pi a}{(b-a)}\sqrt{n_f^2 - (n+\Delta n)^2} - \Delta l\Big],$$

#207917 - $15.00 USD Received 10 Mar 2014; revised 12 Apr 2014; accepted 29 Apr 2014; published 9 May 2014

where ceil stands for the integer obtained by rounding upward. Since the minimum value l has to be ≥ 1, we set $l_{\min}$ as $\max\{1, g\}$.

3.3. *Calculation of $S^{zz}_{\Delta n}$ and $\Omega^{zz}_{\Delta n}$*

The final step is to calculate $S^{zz}_{\Delta n}$ and $\Omega^{zz}_{\Delta n}$ as defined in Eq. (12). Recalling that $\Delta\nu = \Delta n$ and that each sum involves all three quantum numbers, we can write $S^{zz}_{\Delta n}$ as,

$$S^{zz}_{\Delta n} = \sum_{n=1}^{n_{\max}} \sum_{\Delta l=-1}^{1} \sum_{l=l_{\min}}^{l_{\max}} \sum_{\substack{-l\leq m\leq l \\ m\neq 0}} \sum_{\Delta m} S^{zz}_{n,\Delta n,l,\Delta l,m,\Delta m}.$$

The five-fold term can not be done analytically. However, we can reduce it to a double sum over n and l by performing the sums over m and Δm analytically. Further, terms with $\delta_{\Delta n,0}\delta_{\Delta l,0}$ and $\delta_{\Delta n,0}\delta_{\Delta l,-1}$, that imply no change in energy level and energy emission respectively are neglected since we are considering transitions that result only in absorption. The result is found to be

$$\begin{aligned} S^{zz}_{\Delta n} = \sum_{n=1}^{n_{\max}} \sum_{\Delta l=-1}^{1} \sum_{l=l_{\min}}^{l_{\max}} \frac{3(b-a)^2}{4\pi^2 k_1^2 a^2 n_f^3} \Big\{ \frac{l(5+9l+4l^2)}{3(3+8l+4l^2)} \Big[H + \frac{2(l+1)(b-a)^2 H}{\pi^2 a^2 (2n+\Delta n)\Delta n} \\ + 2(l+1)\frac{b^2}{a^2}\delta_{\Delta n,0} \Big] \delta_{\Delta l,1} + \frac{l(1+3l-4l^2)}{3(1-4l^2)} \Big[H - \frac{2l(b-a)^2 H}{\pi^2 a^2 (2n+\Delta n)\Delta n} \Big] \delta_{\Delta l,-1} \\ + 2lk_2^2 H \delta_{\Delta l,0} \Big\}, \end{aligned} \tag{32}$$

where,

$$H(n,\Delta n) = \frac{16[(-1)^{\Delta n}-1]^2 n^2 (n+\Delta n)^2}{\pi^2 (2n+\Delta n)^3 \Delta n^3}.$$

Similarly, we can calculate $\Omega^{zz}_{\Delta n}$ using Eq. (31) and (13). The result is found to be

$$\Omega^{zz}_{\Delta n} = \frac{1}{S^{zz}_{\Delta n}} \sum_{n=1}^{n_{\max}} \sum_{\Delta l=-1}^{1} \sum_{l=l_{\min}}^{l_{\max}} S^{zz}_{\Delta n} \frac{\hbar}{2\mu} \left[\frac{\Delta n(2n+\Delta n)\pi^2}{(b-a)^2} + \frac{\Delta l(2l+\Delta l+1)}{a^2} \right]. \tag{33}$$

The dielectric function for the spherical dome shell can now be calculated by substituting Eq. (32) and (33) in Eq. (12).

4. Results and discussion

In this section we calculate the real and imaginary parts of the dielectric function as a function of wavelength for a practical configuration of a metallic dome shell. We choose silver (Ag) as the shell material owing to the availability of a wide range of data for this metal. Using Eq. (32) and (33) we calculate the dielectric functions of a dome with a fixed cut-off angle and compared it to that of a complete shell (Appendix 5). We also compare it to the Drude model with size-dependent correction as given in Eqs. (1) and (2). Since the cut-off angle we consider are relatively small, we assume that the effective mean free path of the electron can be approximated by its value for a complete shell [29], i.e., $L_{\text{eff}} = (b-a)$. For similar reasons, we used $A = 1$ in the calculations [34]. Values of ω_p and γ_{bulk} were taken as 8.97 eV and 0.016 eV, respectively [17]. Fermi energy of the metal was calculated using $E_{\text{Fermi}} = \frac{1}{2}\mu v_f^2$, and Fermi velocity was taken as $v_f = 1.39 \times 10^6\,\text{ms}^{-1}$ for Ag [17].

The wavelength range we are interested in corresponds to 300 to 1200 nm. Interband component ($\varepsilon_{\text{inter}}$) of the dielectric function for Ag does not have a significant variation with size when dimensions are above 2 nm [30]. This allows us to use the following size-independent

#207917 - $15.00 USD Received 10 Mar 2014; revised 12 Apr 2014; accepted 29 Apr 2014; published 9 May 2014

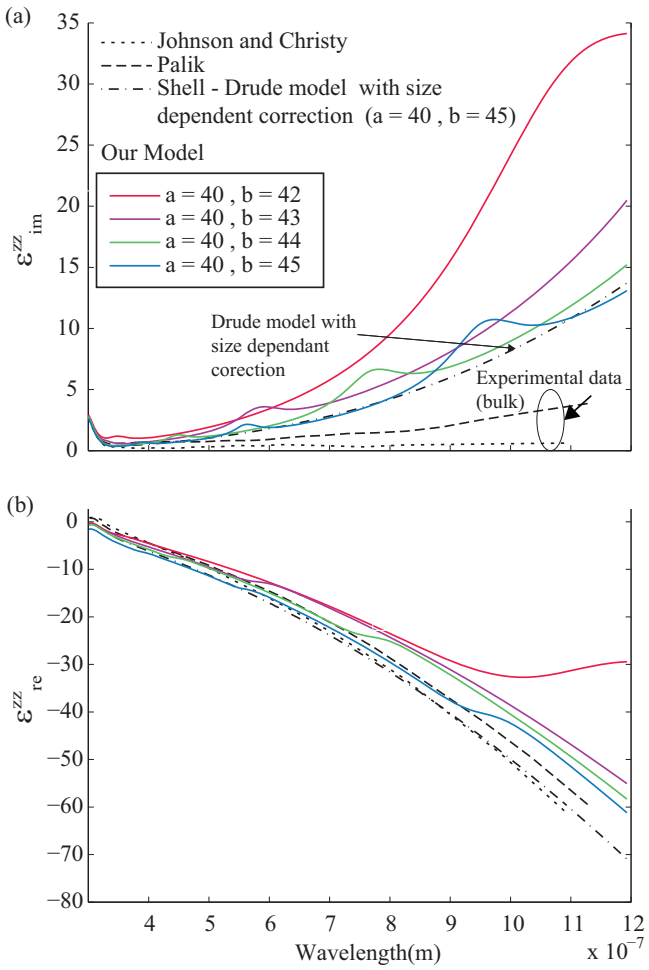

Fig. 2. Imaginary (a) and real (b) parts of the dielectric functions of spherical dome shells of varying thickness calculated with the quantum mechanical model are shown by solid lines. Cut-off angle is 25.8° ($\zeta = 0.9$) for the spherical dome shells. Empirical values obtained from Drude model with size dependent correction for a shell with $a = 40$ nm and $b = 45$ nm is shown by the dotted-dashed line. a and b values given in the figure are in nanometers. The dashed line and dotted line shows the experimental bulk dielectric values taken from Refs. [27] and [38] respectively.

interband term in our permittivity model, which matches with the experimental bulk data for this frequency range [17],;

$$\varepsilon_{\text{inter}}(\omega) = \frac{3.66}{1 - \exp(4.08 - \hbar\omega/q_e)} - 1.$$

Calculated dielectric functions of spherical Ag dome shells of four different thickness (2 to 5 nm) are shown in Fig. 2. It can be seen that oscillatory behaviour of the dielectric function is highly dependent on the thickness of the spherical dome shell. The dot-dashed line shows the results of the Drude model with size dependent correction for a shell with $a = 40$ nm and $b = 45$ nm. It provides a reasonable approximation to the blue curve obtained numerically but

#207917 - $15.00 USD Received 10 Mar 2014; revised 12 Apr 2014; accepted 29 Apr 2014; published 9 May 2014

fails to reproduce oscillations seen there. Also when the thickness is increased, the quantum-mechanical dielectric function of the spherical dome shell gets closer to the experimental bulk data values.

Behaviour of the dielectric function as we change the cut-off angle is shown by Fig. 3. It can be seen that the imaginary part of the dielectric function increases slightly with a decreasing cut-off angle. Also we can see that the quantum mechanical dielectric function of the spherical shell begins approaching that of a spherical dome shell for the smallest cut-off angle. When the cut-off angle is reduced to zero, dielectric function of the spherical dome shell we have derived should match that of the spherical shell. For this, we have to include the $l = 0$ and $m = 0$ terms we discarded in the calculations while calculating $S^{zz}_{\Delta n}$ and $\Omega^{zz}_{\Delta n}$ since the boundary condition for a spherical dome shell given in given in Eq. (22) is not relevant for a complete shell.

It is evident from the Figs. 2 and 3 that the influence of varying the shell thickness is much stronger than varying the cut-off angle on the dielectric function of spherical dome shells. This is because the quantum confinement is much stronger in the radial direction than in the polar direction for the spherical dome shells we have considered here.

Also, it is apparent from Figs. 2 and 3 that the quantum-mechanical dielectric function can exhibit oscillatory behavior for some parameter values, a feature absent from the Drude model even when size dependent corrections are included. The origin of oscillation lies in the quantization of the energy levels, which clearly cannot be included within the framework of the Drude model. It can be seen from the expression for the energy levels of an electron [Eq. (18)] that, because of the term $(b-a)^2$ in the denominator of the first term, for thin spherical dome shells energy difference between different states with different n values is large and therefore cannot be ignored, as is done in classical models by replacing the sum by an integral. In other words, when the oscillator strength weighted average transition frequency, $\Omega^{zz}_{\Delta v}$, is close to the frequency of the incident electric field, the polarizability of the particle increases substantially and results in distinctive peaks in the dielectric function.

Similar oscillatory behavior due to quantum confinement has been experimentally observed for material properties such as conductivity in literature [20, 21].

Calculated extinction cross section of a spherical dome shell using our model and the Drude model with size dependant correction are shown in Fig. 4. It can be seen that the oscillations in the quantum mechanically derived dielectric function will create variations in the extinction spectrum as well.The position of oscillations in the dielectric function and therefore, the corresponding variations in the extinction spectrum depends on the thickness, aspect ratio and cut off angle of the spherical dome shell. In Fig. 4, such variations can be seen in the wavelength range 500 - 600 nm and 900 - 1100 nm. Based on these geometric parameters, if dominant oscillations occur close to the plasmon resonance frequency, it can shift or broaden the plasmon resonance in the extinction spectrum. Knowledge of such variations become important for sensitive sensing applications such as SERS.

In addition to quantum size effects, interband effects and surface scattering we have discussed here, dielectric functions of nano particles exhibit nonlocal effects related to in-homogeneous distribution of surface electrons and electron spill-outs.

In Ref. [17], experimental EELS data for Ag nanospheres with dimensions in 1–10 nm range has been well matched by a theoretical model which was developed by considering contributions to the dielectric function from screening effects due to d-electrons (inter band contributions), surface scattering and discretization electronic energy levels (quantum size effects). This model is very much similar to the model we have developed here. In the Ref. [39], in addition to contributions from inter band effects and quantum size effects, nonlocal effects including electron spill-outs are considered to exlain experimental data of Ref. [17] for Ag spheres. However, in Ref. [39] they employ a much simpler model, that does not reflect energy gap differ-

#207917 - $15.00 USD Received 10 Mar 2014; revised 12 Apr 2014; accepted 29 Apr 2014; published 9 May 2014

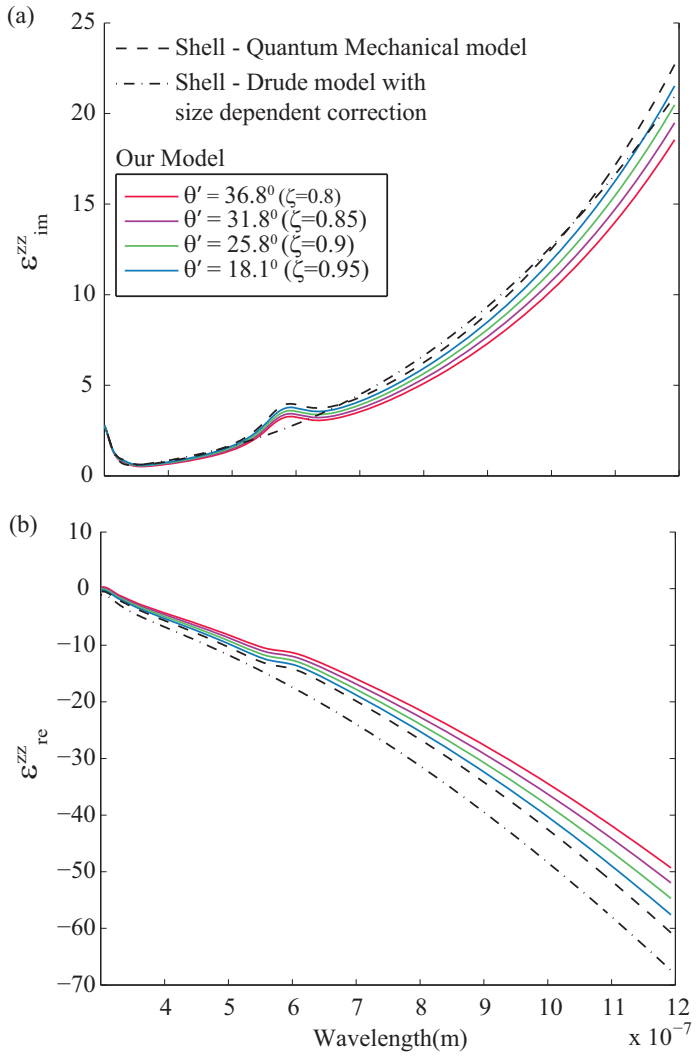

Fig. 3. Imaginary (a) and real (b) parts of the dielectric function of spherical dome shells for four different cut-off angles (solid lines). The dielectric function of a complete shell ($\theta' = 0$) calculated with the quantum-mechanical model is shown by a dashed line, while values obtained from the Drude model with size dependent corrections ares shown by a dotted dash line. In all calculations $a = 40\,\text{nm}$ and $b = 43\,\text{nm}$.

ences between different electronic levels, to obtain the quantum size effects. The calculations in Ref. [17] seem to show strong agreement with experimental data, even without nonlocal effects including electron spill-outs. Electron spill-outs result in red shifts in resonance energy. Also, it has been shown that nonlocal effects [40, 41] on the dielectric function can become significant for nanoshells [42] when the outer radius of the shells becomes very small (10 nm) or when the shell thickness becomes very small (1 nm). They become less significant with the increasing shell radius, even though the thickness is small. Since the dome shell diameter we are considering is much greater than 10 nm and thickness is >1 nm, we do not consider the these effects on the dielectric function in our analysis.

#207917 - $15.00 USD Received 10 Mar 2014; revised 12 Apr 2014; accepted 29 Apr 2014; published 9 May 2014

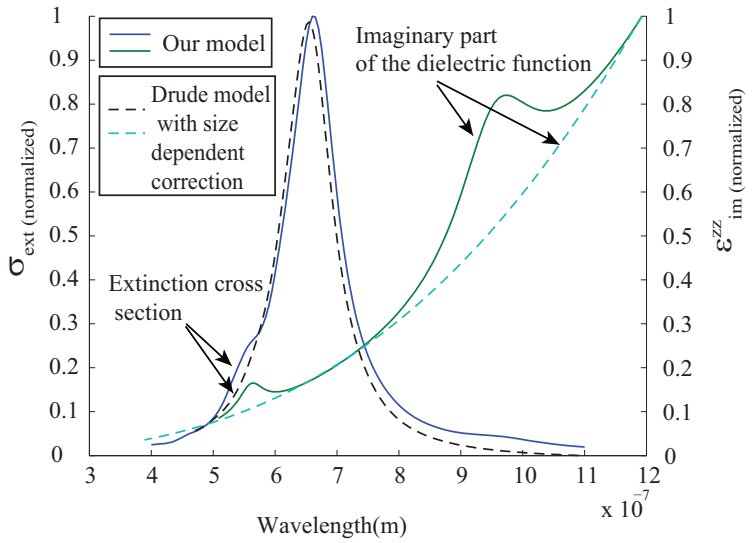

Fig. 4. Extinction cross section and the imaginary part of the dielectric functions of a spherical dome shell calculated using our model and the Drude model with size dependent correction. The dimensions are $a = 40\,\text{nm}$, $b = 45\,\text{nm}$ and cut-off angle $= 25.8^\circ$ ($\zeta = 0.9$). For extinction cross section calculations, the core of the spherical dome shell was taken as Si ($\varepsilon = 2.04$) and the surrounding as air ($\varepsilon = 1$).

5. Conclusions

We have obtained the quantized energy levels and the corresponding wave functions of a free electron inside a spherical dome shell. We used them to calculate the dielectric function of such a dome shell with the assumption of a small cut-off angle using shifted associated Legendre polynomials. We have compared our results with the classical Drude model, modified to include size-dependent corrections, and also with the experimental bulk permittivity data. We have also compared the spherical dome shell with its spherical shell counterpart using a fully quantum-mechanical analysis to study how much the removal of a small part of the shell effects the results.

Oscillatory behaviour seen in the dielectric function is due to the presence of discreet energy levels in our calculations, which cannot be ignored for small dimensions. When the diameter of the spherical dome shell is large while the cut-off angle is small, the quantum confinement is much higher in the radial direction than in the polar direction, and the quantum-mechanical dielectric function of the shell can be taken as a close approximation to that of a spherical dome shell. The Drude model including the size dependent correction also provides a close approximation in the frequency range we have considered, particularly when the oscillations become negligible as the thickness of the spherical dome shell is increased.

Oscillatory behavior seen in the dielectric function will cause variations in the extinction spectrum in the corresponding wavelength range.

The quantum mechanical dielectric function derived in this paper is based on the behaviour of a non-interacting electron gas confined within a thin spherical-shape dome shell. Our results provide an insight into how the quantum effects introduce the geometric parameters into the dielectric function of thin spherical dome shells, at a tolerable computational cost. Study of

#207917 - $15.00 USD Received 10 Mar 2014; revised 12 Apr 2014; accepted 29 Apr 2014; published 9 May 2014

such quantum effects for particles of different shapes are extremely useful for engineering real world applications such as quantum cryptography, energy harvesters, transistor, lasers, quantum computers, quantum communication systems etc. Spherical dome shells with their unique optical properties can offer new opportunities in the design of these applications.

Appendix A: properties of $\widetilde{P}_l^m(x)$

We can prove the orthogonality of the shifted associated Legendre polynomials, $\widetilde{Q}_l^m(x)$, as follows. Let $\acute{x} = k_1 x + k_2$. From Eq. (29) and (24) we can write

$$\begin{aligned}
\int_{-1}^{\zeta} \widetilde{Q}_l^m(x)\widetilde{Q}_{l'}^m(x)dx &= \int_{-1}^{\zeta} \sqrt{k_1 \frac{(2l+1)(l-m)!}{2(m+l)!}}\widetilde{P}_l^m(x) \sqrt{k_1 \frac{(2l'+1)(l'-m)!}{2(m+l')!}}\widetilde{P}_{l'}^m(x)dx \\
&= \sqrt{k_1 \frac{(2l+1)(l-m)!}{2(m+l)!}} \sqrt{k_1 \frac{(2l'+1)(l'-m)!}{2(m+l')!}} \frac{1}{k_1} \int_{-1}^{1} P_l^m(\acute{x})P_{l'}^m(\acute{x})d\acute{x} \\
&= \sqrt{k_1 \frac{(2l+1)(l-m)!}{2(m+l)!}} \sqrt{k_1 \frac{(2l'+1)(l'-m)!}{2(m+l')!}} \frac{1}{k_1} \frac{2(m+l)!}{(2l+1)(l-m)!}\, \delta_{l,l'} \\
&= k_1 \frac{(2l+1)(l-m)!}{2(m+l)!} \frac{1}{k_1} \frac{2(m+l)!}{(2l+1)(l-m)!}\, \delta_{l,l'} \\
&= 1.
\end{aligned}$$

We can also obtain a recurrence relation for the shifted associated Legendre polynomials. From Eq. (25), (27) and (28), we obtain

$$\begin{aligned}
(l-m)P_l^m(k_1x+k_2) &= (k_1x+k_2)(2l-1)P_{l-1}^m(k_1x+k_2) - (l+m-1)P_{l-2}^m(k_1x+k_2) \\
(l-m)\widetilde{P}_l^m(x) &= (k_1x+k_2)(2l-1)\widetilde{P}_{l-1}^m(x) - (l+m-1)\widetilde{P}_{l-2}^m(x) \\
(k_1x+k_2)(2l-1)\widetilde{P}_{l-1}^m(x) &= \frac{(l-m)\widetilde{P}_l^m(x) + (l+m-1)\widetilde{P}_{l-2}^m(x) - k_2(2l-1)\widetilde{P}_{l-1}^m(x)}{k_1(2l-1)}. \quad (34)
\end{aligned}$$

Appendix B: calculation of the matrix element M_{if}

The matrix element in Eq. (30) can be written explicitly as,

$$\begin{aligned}
M_{if} &= \int_0^{2\pi}\int_{\theta'}^{\pi} \left\{ \sin\theta\cos\theta Q(\theta)_{l,m}[Q(\theta)_{l+\Delta l,m+\Delta m}]^* F(\phi)_m[F(\phi)_{m+\Delta m}]^*\, d\theta d\phi \right\} \times \\
&\quad \int_a^b r^3 R(r)_{n,l}[R(r)_{n+\Delta n,l+\Delta l}]^*\, dr. \quad (35)
\end{aligned}$$

The integration involving the radial part is the same as for a spherical shell and can be performed as [36],

$$\int_a^b r^3 R(r)_{n,l}[R(r)_{n+\Delta n,l+\Delta l}]^*\, dr = \frac{4(b-a)[(-1)^{\Delta n}-1]n(n+\Delta n)}{\pi^2(2n+\Delta n)^2\Delta n^2} + b\delta_{\Delta n,0}.$$

The remaining part of the integration, which involves the polar and azimuthal components is different from a spherical shell. It can be calculated using expressions derived for $F(\phi)$ and

#207917 - $15.00 USD Received 10 Mar 2014; revised 12 Apr 2014; accepted 29 Apr 2014; published 9 May 2014

$Q(\theta)$ in Eq. (29) and (20) as follows.

$$\begin{aligned}
&\int_0^{2\pi}\int_{\theta'}^{\pi} \sin\theta\cos\theta Q(\theta)_{l,m}[Q(\theta)_{l+\Delta l,m+\Delta m}]^* F(\phi)_m [F(\phi)_{m+\Delta m}]^*\, d\theta d\phi \\
&= \sqrt{k_1\frac{(2l+1)(l-m)!}{2(m+l)!}}\sqrt{k_1\frac{[2(l+\Delta l)+1][(l+\Delta l)-(m+\Delta m)]!}{2[(m+\Delta m)+(l+\Delta l)]!}} \\
&\quad \int_0^{2\pi}\frac{1}{\sqrt{2\pi}}\exp(jm\phi)\frac{1}{\sqrt{2\pi}}\exp[-i(m+\Delta m)\phi]d\phi \\
&\quad \int_{\theta'}^{\pi}\sin\theta\cos\theta\widetilde{P}_l^m(\cos\theta)\widetilde{P}_{l+\Delta l}^{m+\Delta m}(\cos\theta)\, d\theta \\
&= \delta_{\Delta m,0}\sqrt{k_1\frac{(2l+1)(l-m)!}{2(m+l)!}}\sqrt{k_1\frac{[2(l+\Delta l)+1][(l+\Delta l)-m]!}{2[m+(l+\Delta l)]!}} \\
&\quad \int_{\theta'}^{\pi}\sin\theta\cos\theta\widetilde{P}_l^m(\cos\theta)\widetilde{P}_{l+\Delta l}^{m}(\cos\theta)\, d\theta \\
&= \delta_{\Delta m,0}\sqrt{k_1\frac{(2l+1)(l-m)!}{2(m+l)!}}\sqrt{k_1\frac{[2(l+\Delta l)+1][(l+\Delta l)-m]!}{2[m+(l+\Delta l)]!}}\int_{-1}^{\zeta} x\widetilde{P}_l^m(x)\widetilde{P}_{l+\Delta l}^{m}(x)\, dx.
\end{aligned} \tag{36}$$

After substituting the recurrence relation given by Eq. (34) in (36), this can be further simplified as,

$$\begin{aligned}
&\int_0^{2\pi}\int_{\theta'}^{\pi} \sin\theta\cos\theta Q(\theta)_{l,m}[Q(\theta)_{l+\Delta l,m+\Delta m}]^* F(\phi)_m [F(\phi)_{m+\Delta m}]^*\, d\theta d\phi \\
&= \delta_{\Delta m,0}\sqrt{k_1\frac{(2l+1)(l-m)!}{2(m+l)!}}\sqrt{k_1\frac{[2(l+\Delta l)+1][(l+\Delta l)-m]!}{2[m+(l+\Delta l)]!}}\times \\
&\quad \int_{-1}^{\zeta}\Big\{\frac{[(l+1)-m]\widetilde{P}_{l+1}^m(x)+[(l+1)+m-1]\widetilde{P}_{(l+1)-2}^m(x)-k_2[2(l+1)-1]\widetilde{P}_{(l+1)-1}^m(x)}{k_1[2(l+1)-1]}\times \\
&\quad \widetilde{P}_{l+\Delta l}^m(x)\Big\}\, dx \\
&= \delta_{\Delta m,0}\Big[\sqrt{\frac{(l+1+m)(l+1-m)}{(2l+1)(2l+3)}}\frac{\delta_{\Delta l,1}}{k_1}+\sqrt{\frac{(l+m)(l-m)}{(2l-1)(2l+1)}}\frac{\delta_{\Delta l,-1}}{k_1}-\frac{k_2}{k_1}\delta_{\Delta l,0}\Big].
\end{aligned}$$

Therefore, we can write M_{if} as,

$$\begin{aligned}
M_{if} &= \Big\{\frac{4(b-a)[(-1)^{\Delta n}-1]n(n+\Delta n)}{\pi^2(2n+\Delta n)^2\Delta n^2}+b\delta_{\Delta n,0}\Big\}\times \\
&\quad \delta_{\Delta m,0}\Big[\sqrt{\frac{(l+1+m)(l+1-m)}{(2l+1)(2l+3)}}\frac{\delta_{\Delta l,1}}{k_1}+\sqrt{\frac{(l+m)(l-m)}{(2l-1)(2l+1)}}\frac{\delta_{\Delta l,-1}}{k_1}-\frac{k_2}{k_1}\delta_{\Delta l,0}\Big]
\end{aligned}$$

#207917 - $15.00 USD Received 10 Mar 2014; revised 12 Apr 2014; accepted 29 Apr 2014; published 9 May 2014

Appendix C: quantum mechanical dielectric function for shell

The terms $S^{zz}_{\Delta n}$ and $\Omega^{zz}_{\Delta n}$ for a spherical shell of small thickness can be given as [36],

$$
\begin{aligned}
S^{zz}_{\Delta n} &= \sum_{n=1}^{n_{\max}} \sum_{l=l_{\min}}^{l_{\max}} \sum_{\Delta l=-1}^{1} \Bigg(\Big\{ \frac{4(b-a)^2[(-1)^{\Delta n}-1]^2 n^2 (n+\Delta n)^2 (l+1)}{\pi^4 a^2 n_f^3 (2n+\Delta n)^3 \Delta n^3} \\
&\quad + \frac{8(b-a)^4[(-1)^{\Delta n}-1]^2 n^2 (n+\Delta n)^2 (l+1)^2}{\pi^6 a^4 n_f^3 (2n+\Delta n)^4 \Delta n^4} + \frac{(b-a)^2 (l+1)^2}{a^2 \pi^2 n_f^3} \delta_{\Delta n,0} \Big\} \delta_{\Delta l,+1} \\
&\quad + \Big\{ \frac{4(b-a)^2[(-1)^{\Delta n}-1]^2 n^2 (n+\Delta n)^2 l}{\pi^4 a^2 n_f^3 (2n+\Delta n)^3 \Delta n^3} - \frac{8(b-a)^4[(-1)^{\Delta n}-1]^2 n^2 (n+\Delta n)^2 l^2}{\pi^6 a^4 n_f^3 (2n+\Delta n)^4 \Delta n^4} \Big\} \delta_{\Delta l,-1} \Bigg) \\
\Omega^{zz}_{\Delta n} &= \frac{1}{S^{zz}_{\Delta n}} \sum_{n=1}^{n_{\max}} \sum_{l=l_{\min}}^{l_{\max}} \sum_{\Delta l=-1}^{1} S^{zz}_{\Delta n} \frac{\hbar}{2\mu} \left[\frac{\Delta n (2n+\Delta n)\pi^2}{(b-a)^2} + \frac{\Delta l (2l+\Delta l+1)}{a^2} \right].
\end{aligned}
$$

where,

$$
\begin{aligned}
n_{\max} &= \left[\left[\sqrt{\frac{2\mu}{\hbar^2} \left[\frac{(b-a)^2 E_{\text{Fermi}}}{\pi^2} \right]} \right] \right], \\
l_{\max} &= \left\lfloor \frac{\pi a}{(b-a)} \sqrt{(n_f^2 - n^2)} \right\rfloor, \\
l_{\min} &= \max\{0, \left\lceil \frac{a\pi}{(b-a)} \sqrt{n_f^2 - (n+\Delta n)^2} - \Delta l \right\rceil \}.
\end{aligned}
$$

Acknowledgments

The work of C.S Kumarasinghe is supported by the Monash University Institute of Graduate Research. The work of M. Premaratne and G.P Agrawal are supported by the Australian Research Council, through its Discovery Grants DP110100713 and DP140100883.

#207917 - $15.00 USD Received 10 Mar 2014; revised 12 Apr 2014; accepted 29 Apr 2014; published 9 May 2014